

# UC Irvine

## UC Irvine Previously Published Works

### Title

A methodological pipeline for serial-section imaging and tissue realignment for whole-brain functional and connectivity assessment.

### Permalink

<https://escholarship.org/uc/item/7wt826jp>

### Authors

Mesina, Lilia  
Wilber, Aaron A  
Clark, Benjamin J  
et al.

### Publication Date

2016-06-01

### DOI

10.1016/j.jneumeth.2016.03.021

Peer reviewed



Published in final edited form as:

*J Neurosci Methods*. 2016 June 15; 266: 151–160. doi:10.1016/j.jneumeth.2016.03.021.

## A Methodological Pipeline for Serial-Section Imaging and Tissue Realignment for Whole-brain Functional and Connectivity Assessment

Lilia Mesina<sup>1,\*</sup>, Aaron A. Wilber<sup>1,2,\*</sup>, Benjamin J. Clark<sup>3,\*</sup>, Sutherland Dube<sup>1</sup>, Alexis J. Demecha<sup>1</sup>, Craig E. L. Stark<sup>2</sup>, and Bruce L. McNaughton<sup>1,2</sup>

<sup>1</sup>Canadian Centre for Behavioural Neuroscience, The University of Lethbridge, Lethbridge, AB, Canada

<sup>2</sup>Department of Neurobiology and Behavior, University of California, Irvine, CA, USA

<sup>3</sup>Department of Psychology, The University of New Mexico, Albuquerque, NM, USA

### Abstract

**Background**—Understanding the neurobiological basis of cognition and behavior, and disruptions to these processes following injury and disease, requires a large-scale assessment of neural populations, and knowledge of their patterns of connectivity.

**New Method**—We present an analysis platform for large-scale investigation of functional and neuroanatomical connectivity in the rodents. Retrograde tracers were injected and in a subset of animals behavioral tests to drive immediate-early gene expression were administered. This approach allows users to perform whole-brain assessment of function and connection in a semi-automated quantitative manner. Brains were cut in the coronal plane, and an image of the block face was acquired. Wide-field fluorescent scans of whole sections were acquired and analyzed using Matlab software.

**Results**—The toolkit utilized open-source and custom platforms to accommodate a largely automated analysis pipeline in which neuronal boundaries are automatically segmented, the position of segmented neurons are co-registered with a corresponding image acquired during vibratome sectioning, and a 3-D representation of neural tracer (and other products) throughout the entire brain is generated.

**Comparison with Existing Methods**—Current whole brain connectivity measures primarily target mice and use anterograde tracers. Our focus on segmented units of interest (e.g., NeuN labeled neurons) and restricting measures to these units produces a flexible platform for a variety of whole brain analyses (measuring activation, connectivity, markers of disease, etc.).

\* **Corresponding Authors:** Lilia Mesina, lilia.mesina@uleth.ca, Aaron Wilber, awilber@uci.edu, Benjamin Clark, bnjclark@unm.edu.

**Publisher's Disclaimer:** This is a PDF file of an unedited manuscript that has been accepted for publication. As a service to our customers we are providing this early version of the manuscript. The manuscript will undergo copyediting, typesetting, and review of the resulting proof before it is published in its final citable form. Please note that during the production process errors may be discovered which could affect the content, and all legal disclaimers that apply to the journal pertain.

**Conclusions**—This open-source toolkit allows an investigator to visualize and quantify whole brain data in 3-D, and additionally provides a framework that can be rapidly integrated with user-specific analyses and methodologies.

### Keywords

connectome; immediate-early genes; Neuroimaging; Functional networks; Neural tracing; Tissue Realignment

---

## Introduction

A broad aim of cognitive neuroscience is to understand brain and behavior in terms of the dynamic interaction between populations of neurons, as well as their patterns of connectivity across wide areas of the nervous system (Alivisatos et al., 2012; Sporns, 2014; Van Essen, 2013). The development and refinement of automated methods to systematically quantify the inputs and outputs of pathways spanning whole-brains, and in some cases across entire nervous systems, has been a target of anatomical studies for some time (Leergaard et al., 1995) and these approaches are now widely in use (Chung et al., 2013; Johnson and Frostig, 2015; Oh et al., 2014; Ragan et al., 2012; Watabe-Uchida et al., 2012; Wilber et al., 2015; Zingg et al., 2014). The functional organization of identified networks can additionally be resolved by comparing and co-localizing connectivity data-bases with discrete markers of neuronal activity such as the induction of immediate-early gene expression (Alivisatos et al., 2012; Guzowski et al., 2005; Kim et al., 2015; Vousden et al., 2015). Further, a number of recent studies have combined immediate early gene markers of neural activity with neuroanatomical tracing by using triple-label fluorescence in situ hybridization and immunohistochemistry and imaging with distinct colors for gene, tracer, and nuclei (Clark et al., 2013; Petrovich et al., 2005; Zelikowsky et al., 2013). These methods allow a histological readout of the entire activation pattern for behaviorally relevant events across distinct neural networks.

These extensive functional and neuroanatomical data sets have created a pressing need for high throughput analysis tools, in particular, those that accommodate automated detection and display of large-scale connectivity. Here, we describe an analysis platform written in a Matlab framework, which conveniently combines several open-source software platforms such that users may detect, display, and quantify input-output relationships in fluorescent images sampled across entire brains and in 3-D. The methods presented here include image capture and tissue collection procedures that have been previously published, however, these methods will be summarized briefly below (Montes-Rodriguez et al., 2013; Wilber et al., 2015). We demonstrate application of this approach to a variety of data sets including neuroanatomical and functional single cell activation studies in the rat brain, demonstrating that this software tool can be rapidly adapted for analysis of any nervous system marker or stain that has been serially-sectioned and block-face imaged. This Matlab based program is available for download (<https://github.com/lilicamd/BrainSegmenterGUI>).

## Methods and Results

### Subjects

All experiments using neural tracer were performed on 3–15 month male and female Fisher Brown Norway rats (n = 10, 170–430g), the subject for the immediate early gene (IEG) detection experiment was a single 2-month-old male C57 mouse (23.3g), and the subject from the IEG and neural tracer experiment was a 9-month old female Long-Evans rat (250g). All experiments were carried out in accordance with the University of Lethbridge Animal Welfare Committee and conformed to NIH Guidelines on the Care and Use of Laboratory Animals.

### Neuroanatomical tracers and microinjection surgery

Details for the neuroanatomical data collection and analyses were presented previously and methodological details can be found here (Wilber et al., 2015). In addition, these methods are summarize briefly below. Each animal received a unilateral microinjection of either a retrograde or an anterograde tracer into the parietal cortex (PC). The fluorescent retrograde tracers, cholera toxin-B Alexa Fluor conjugate 594 (CTB; 1% in Phosphate Buffered Saline 0.1 M; Life Technologies, Burlington, ON) and Fluoro-Gold (FG; 4% in Phosphate Buffered Saline 0.1 M; Fluorochrome, Denver, CO) were used to map inputs to dorsal and ventral cortical regions. The injection location in dorsal cortex varied across rats to provide rostral-caudal coverage of the areas traditionally characterized as PC (MPta and LPta, respectively; Paxinos and Watson, 2007) and the area previously characterized as medial secondary visual cortex (V2MM and V2ML, respectively; Paxinos and Watson, 2007), but recently shown to be functionally similar to primate PC (Wilber et al., 2014). In ventral regions, injections targeted the lateral entorhinal cortex (Clark et al., 2013).

### Vibratome sectioning and block-face imaging

After a 14-day survival period, rats were overdosed with euthansol and perfused transcardially with a phosphate buffer solution (pH 7.4) followed by 4% paraformaldehyde (PFA) in Phosphate Buffered Saline 0.1 M (PBS). Brains were extracted and post fixed in PFA 4° C for 24h, then cryoprotected in 30% sucrose (with or without 0.02% sodium Azide). Brains were then embedded in agarose (Agarose-1B, Sigma-Aldrich Canada Co., Oakville, ON) and sectioned in the coronal plane at 50um using a custom vibratome (Model VT1200 S, Leica Biosystems, Concord, ON; with modifications by Peira Scientific Instruments, Belgium). The vibratome was equipped with a camera (mV BlueFOX 121G, 10× lens) mounted above the specimen thereby allowing the acquisition of block-face images for the purpose of registering processed tissue sections and 3D rendering (Figure 1). Alternatively, the same system can be implemented with frozen tissue on a sliding microtome.

Sections were collected in parallel series in PBS. A series was processed with a NeuN antibody conjugated to fluorescent dye (Alexa Fluor 405; Life Technologies, Burlington, ON), mounted in PBS, and cover slipped with Vectashield (Vector Laboratories, Burlington, ON). Tissue was mounted in PBS, dehydrated, cleared, and cover slipped.

## Image acquisition

Rapid image acquisition of entire coronal or sagittal sections was conducted using NanoZoomer whole-slide scanning microscopy (NanoZoomer Digital Pathology RS, Hamamatsu Photonics), which is capable of automatically capturing wide-field multispectral fluorescent images over entire brain sections at high resolution. The objective was focused on the middle of the section in the z-plane and image acquisition was conducted with 40× magnification with a multi band pass filter cube (DAPI/FITC/Texas Red; Figure 2).

## Automated detection of retrograde tracer

A custom software platform was developed in Matlab (Matlab2014b, Mathworks Inc., Natick, MA) which accommodates automated neuronal segmentation and realignment of identified tracer filled cells with serial-section block-face imaging (Figure 3). Matlab serves as the platform of choice for data analysis and it was used as high-level integration language because of the GUI features allowed for efficient coordination of the processing pipeline (Figure 3). For the purposes of detecting and computing the location of each neuron within a section, the software first splits NanoZoomer images into large, but manageable 40× magnification tiles using an open source tool called ndpisplit (Figure 1; <http://www.imnc.in2p3.fr/pagesperso/deroulers/software/ndpitools/>). Nearly all of the steps described here are coordinated via the Matlab interface (Figure 4). In other words, Matlab is used to call the executables for ndpisplit, Miji and FARSIGHT (see below). The NDP images are saved to TIF format with no compression and then processed as TIF images thereafter. Sometimes the 40× images were preprocessed outside of Matlab in ImageJ by selectively cropping regions of brain tissue in which the fluorescent staining and imaging was poor. This procedure was performed because segmentation of poorly stained material was not possible without sufficient computational resources. Second, we split images into the appropriate color channels of interest by utilizing the open source image processing software, Fiji (Schindelin et al., 2012; <http://fiji.sc/Fiji>) which was executed using (Sage et al., 2012; <http://fiji.sc/Miji>), a compatibility layer for running ImageJ/Fiji within Matlab. Next, neurons were automatically identified within each 40× tile using ([www.farsight-toolkit.org](http://www.farsight-toolkit.org); Bjornsson et al., 2008; Rey-Villamizar et al., 2014). A detailed description of the algorithms behind the automated nuclei detection has been provided elsewhere (Al-Kofahi et al., 2010), and validation of this tool was provided in our previous work by demonstrating that segmentation was highly correlated with manual verification of neuronal nuclei (Wilber et al., 2015). The average number of detected NeuN labeled neurons in neocortex was 50,214.5 per section and the average number of tracer filled cells per section was of 195.4.

Finally, the automated segmentation of neurons allows for measurement of the precise x-y-position of each neuron, as well as the intrinsic neuronal features including the integrated intensity, i.e., the sum of the pixel intensity values within the segmented boundaries of a neuron for DAPI, FITC, and Texas Red, and the maximum and minimum pixel intensity for each segmented neuron. Based on these measures, we classified neurons as containing retrograde tracer if the total integrated intensity exceeded 250,000, and had a maximum pixel intensity exceeding 150 (individual pixel intensity ranged from 0–255). The user has the option to specify their own parameters in order to optimize the process for their specific application and stains. The Figure 4 shows a snapshot of the Matlab GUI with example from

processing a whole brain section. The accuracy of this criterion was validated by correlating estimates of the number of tracer positive cells within a tissue section, with measures obtained from manual) in Fiji ( $p < 0.01$ ; see Wilber et al., 2015). The Matlab interface allows users the option to validate their own data by applying identical contours for automatic cell counts as were used for manual cell counts in Fiji (Figure 2; [http://fiji.sc/Cell\\_Counter](http://fiji.sc/Cell_Counter)).

In addition to the segmentation methods described above, the software produces a wide-field ( $2.5\times$  magnification) image of the entire tissue section. This low-resolution image can be used to identify specific neuroanatomical boundaries for analyses based on regions of interest (ROIs). Identification of ROIs is facilitated by additional series of tissue sections stained with Cresyl violet and parvalbumin (see Figure 1). The user also has the option to create whole brain cortical flat maps as described previously (Wilber et al., 2015) and briefly summarized here. To generate cortical flat maps, first 2D maps are generated. Our aim with these flattened cortical maps is to conveniently illustrate the anatomical position of identified cells positive for a marker of interest for the entire cortical mantle. Following marker positive cell identification, the matlab interface allows the user to automatically map the position of labeled cells onto a reference line manually drawn through the cortical boundary between layers IV and V. The reference line is automatically smoothed using the 'runline' function of the Chronux data analysis toolbox in Matlab ([www.chronux.org](http://www.chronux.org); Mitra and Bokil, 2007), which implements a moving-window line regression with a window size of 5 pixels ( $1.15\ \mu\text{m}$ ) and a step size of 1 pixel ( $0.23\ \mu\text{m}$ ). Each reference line can be automatically aligned to two user-defined points of interest. We used the lateral border of the cingulate cortex and the location of the rhinal sulcus. These files are marked in ImageJ and saved as a line that is loaded using our Matlab interface to provide cortical reference points for normalizing the position of data. The user can mark additional anatomical boundaries in the same manner as the rhinal sulcus.

### Registration to Block Face Image

Next, we set out to implement methods that allow re-alignment of detected tracer positive cells to a corresponding block-face image (Figure 2) taken during tissue sectioning. Because segmentation is conducted on tissue that has been processed with free-floating immunohistochemistry, the sections are typically distorted when mounted onto slides, and the segmented neuronal coordinates fail to align to their precise anatomical position on the block-face series. To accomplish re-alignment, we first used ImageJ to apply a mask to the block-face series to prevent interference from material that is visible through the agarose and below the section of interest. Next, we took the reduced resolution image of each fluorescently processed tissue section (which is automatically generated by our Matlab GUI) and performed a vector field based registration to map this image onto the block face image using ANTS (Avants et al., 2008; Klein et al., 2009; <http://stnava.github.io/ANTs/>). The steps described in this section are completed in ANTs using the code posted to github (see Figure 3; <https://github.com/lilicamd/MethodsSpace/>). ANTs allows for high-dimensional registration with error metrics like mutual information that are well-suited to images with highly varying contrast profiles (Figure 6). The ANTs code converts all images to Nifti format (with virtually no lag) and performs all image processing in this format. This method

performed well when registering the edges of tissue section; however, we occasionally observed mis-alignment of internal areas of each section, especially within the hippocampus and near ventricular regions. Thus, in order to improve registration of these internal areas of the section, on an ‘as needed’ basis we manually selected points in each section using ITKsnap (<http://www.itksnap.org/>). The registration then began with an affine based solely on the points to provide an initial alignment and continued with a vector-based registration that integrated both grayscale intensity mutual information and point spread estimate error metrics. For sections with missing tissue, or where one hemisphere was mounted in the flipped orientation, we applied a mask to process the appropriate tissue individually. Finally, a pixel based scaling transformation was used to map the tracer positive cell positions from the high-resolution image to the corresponding point on the lower resolution block face image. Anatomical data were then represented on the block face image in two ways: 1) each tracer positive cell was represented as a single colored pixel, which is useful for quantitative analyses (Figure 6 top), and 2) each tracer positive cell was represented as a large symbol that could be easily visualized (Figure 7 bottom). The larger marker format allows users to more easily scroll through the data for subjective assessment of the distribution of labeled cells. The single colored pixel method is ideal for data analyses and quantification because both the precise location of a “positive” cell and the number of positive cells (as pixels) are all directly available in high resolution and in the single image file for the tissue section. For example, a count of the number of red pixels corresponds to the number of tracer positive cells. Further, for functional connectivity analyses, counts of green pixels could correspond to immediate early gene positive cells and counts of yellow pixels could correspond to the number of cells that were positive for both immediate early gene activation and tracer.

### 3D Rendering

Finally, individual sections were extruded in the z-plane to match the section thickness (50um) and allow rendering of data in 3D using Vaa3D, an open source visualization and analysis software package (<http://home.penglab.com/proj/vaa3d/home/index.html>; Peng et al., 2014a; Peng et al., 2014b). This toolkit allows 3D rendering and analysis of very large data sets. We chose to subsample (i.e., processed a subset of the sections for tracer or IEG), therefore we randomly distributed the tracer or IEG markers across a range of sections (though in the case of the IEG data this range did not cover the entire subsampling range which was quite large). For the present analyses anatomical data labeled sections with quantified counts (1:6; Movie 1; <https://github.com/lilicamd/MethodsSpace>) were interspersed with Cresyl violet stained, parvalbumin immunostained and non-quantified tracer labeled sections. Any configuration of stained and/or quantified material could be reconstructed using this method.

### Whole Brain Immediate Early Gene Detection

As a proof of principal for functional connectivity, we performed two additional analyses. First, we conducted an experiment for the detection of the IEG Homer1a on a data set of serial images from a mouse brain. Homer1a and other IEGs (e.g., Arc, Narp, c-Fos) are transcribed rapidly following neuronal firing, and can therefore be used as markers of behaviorally driven ensemble activity following a specific event (Guzowski et al., 1999; Guzowski et al., 2005; Montes-Rodriguez et al., 2013). In the present study, we used

environmental exploration to drive Homer1a expression. The mouse was placed in 3 different novel environments (6min in the first environment and 4min in each of the second and third environments) that differed in visual landmarks and environmental geometry. Following behavior, the mouse was returned to its home cage for approximately 20 minutes in order for sacrifice to coincide with the optimal expression time-point for the IEG Homer1a from the first behavior (Vazdarjanova et al., 2002). Animal sacrifice, vibratome sectioning and block face imaging was done as described above, with the exception that sections were cut at 40um. Fluorescence in situ hybridization (FISH) tissue processing for the detection of Homer1a was performed on one series (every 5th brain section) through hippocampus. Details on the IEG FISH method have been described elsewhere (Guzowski et al., 1999; Montes-Rodriguez et al., 2013; Vazdarjanova et al., 2002). Briefly, tissue was mounted in PBS and dehydrated. A digoxigenin (DIG; Roche) labeled antisense riboprobe targeting the 3' untranslated region (UTR) of mouse Homer1a mRNA was generated in house using PCR. Following probe hybridization (3ng/ul), DIG labeled probes were amplified using a peroxidase-conjugated DIG antibody (1:300; Roche), followed by biotinyl tyramide (1:100; Perkin Elmer) and visualized using a streptavidin Texas-red conjugate (1:200; Perkin Elmer). Sections were then counterstained with 4',6-diamidino-2-phenylindole (DAPI). Image acquisition was done with a NanoZoomer as described above, with the exception that 20x magnification was used. Automated detection of IEG positive cells was performed as described for automated detection of retrograde tracer. Threshold measures to classify cells as Homer1a positive were a total integrated intensity exceeding 57,000, and a maximum pixel intensity exceeding 75. Registration to block face image and 3D rendering were performed as described for tracer experiments (Movie 2; <https://github.com/lilicamd/MethodsSpace>). The average number of detected DAPI labeled cells was 77,339.8 per section and the average number of IEG foci detected per section was 1251.8. The approximate amount of time for processing each section was 5.5h (Note the amount of time can vary dramatically with different computer specifications and in our experience machines with < 40GB of memory did not perform well for these analyses).

The methods and results described above provide support for the use of this software for functional connectomics—that is, 3D maps of retrograde tracer and immediate-early gene expression can be co-registered between brains or within brains (i.e., serial-sections can be processed for IEG or tracer and co-registered). In a second proof-of-principal demonstration, we also show that the FARSIGHT toolbox can accommodate detection of both immediate-early gene expression and tracer within the same tissue sections (i.e., triple fluorescent labeled material; see Figure 8 for experimental design; data from Clark et al., 2013). For instance, individual nuclei (DAPI stain) or neuronal cell bodies (NeuN stain) can be segmented and the integrated intensity for other fluorophores can be measured within or surrounding the segmented objects (see Figure 8B, inset). Thus, experimental procedures combining both IEG with neuroanatomical tracer could make use of the methods described above. Further, because the FARSIGHT can be utilized to segment both NanoZoomer and confocal z-stack images (Fig. 8), it is possible that the procedures above can be flexibly utilized for a diverse set of imaging applications (e.g., wide-field fluorescent images or single layer confocal mosaics). We do not, however, provide a comparison of imaging applications in the present manuscript.



## Conclusions

We describe a custom software platform that accommodates an automated analysis pipeline in which neuronal boundaries are identified and segmented, co-registered with corresponding serial images acquired during tissue sectioning, and a platform for 3-D visualization and analysis of whole brain connectivity data. We illustrate the functionality of this new system with brains collected from rats and mice. It is important to note that our software platform allows for the integration of additional functionality, for example, metrics could be added addressing the informatics problem of dealing with data from a large number of serial sections. Although our framework is focused on the detection of neuronal cell bodies and retrograde tracer, the open-source segmentation software used here (FARSIGHT) can also detect axonal projections and small biological features (Kulkarni et al., 2015; Megjhani et al., 2015; Narayanaswamy et al., 2011). However, our intention was to develop a toolkit that will allow an extension of the analysis pipeline to detect multiple immediate early gene products, which are found within neuronal nuclei, and if tagged with distinct fluorophores, could potentially be co-registered with retrograde tracer allowing an investigator to explore the functional relationships within identified circuits. In addition, the resulting 3D data model can easily be exported to NineML format, a language for efficient model sharing (<http://software.incf.org/software/nineml>). A final consideration is that most of our work was conducted on cortical tissue and CA subregions of the hippocampus, in large part, due to the nature of the tightly packed neurons in the thalamus and dentate gyrus, thereby increasing the number of segmentation errors and manual effort required to correct these errors. In future refinements of our software platform, additional work could be integrated improving the quality of segmentation of NeuN tagged cell bodies, or possibly by testing using other antibody and fluorophore combinations.

## Supplementary Material

Refer to Web version on PubMed Central for supplementary material.

## Acknowledgments

This research was supported by the Alberta Innovates Health Solutions Polaris Award to BLM, a Natural Sciences and Engineering Council of Canada Discovery Grant to BLM, Alberta Innovates Health Solutions Fellowships to AAW and BJC, MH099682 and AG049090 to AAW, a Natural Sciences and Engineering Council of Canada Fellowship to BJC, and an Alberta Innovates Health Solutions Graduate Studentship to SD. The block face imaging system was developed with support from Neuroelectronic Research Flanders (NERF). The authors thank Dr. Majid Mohajerani for providing brain specimens used for immediate-early gene expression analyses, Valérie Lapointe for *in situ* hybridization tissue processing, and Karim Ali, Marina Galatnov and Jarret McKinnon for assistance with analyses.

## References

- Al-Kofahi Y, Lassoued W, Lee W, Roysam B. Improved automatic detection and segmentation of cell nuclei in histopathology images. *IEEE transactions on bio-medical engineering*. 2010; 57:841–52. [PubMed: 19884070]
- Alivisatos AP, Chun M, Church GM, Greenspan RJ, Roukes ML, Yuste R. The brain activity map project and the challenge of functional connectomics. *Neuron*. 2012; 74:970–4. [PubMed: 22726828]

- Avants BB, Epstein CL, Grossman M, Gee JC. Symmetric diffeomorphic image registration with cross-correlation: Evaluating automated labeling of elderly and neurodegenerative brain. *Medical Image Analysis*. 2008; 12:26–41. [PubMed: 17659998]
- Bjornsson CS, Lin G, Al-Kofahi Y, Narayanaswamy A, Smith KL, Shain W, Roysam B. Associative image analysis: a method for automated quantification of 3D multi-parameter images of brain tissue. *J Neurosci Methods*. 2008; 170:165–78. [PubMed: 18294697]
- Chung K, Wallace J, Kim SY, Kalyanasundaram S, Andalman AS, Davidson TJ, Mirzabekov JJ, Zalocusky KA, Mattis J, Denisin AK, Pak S, Bernstein H, Ramakrishnan C, Grosenick L, Gradinaru V, Deisseroth K. Structural and molecular interrogation of intact biological systems. *Nature*. 2013; 497:332–7. [PubMed: 23575631]
- Clark, BJ., Wilber, AA., Witharana, WK., McNaughton, BL. Functional connectivity of three-dimensional object coding in perirhinal-entorhinal circuitry. Poster Society for Neuroscience; San Diego, CA: 2013.
- Guzowski JF, McNaughton BL, Barnes CA, Worley PF. Environment-specific expression of the immediate-early gene *Arc* in hippocampal neuronal ensembles. *Nat. Neurosci*. 1999; 2:1120–4. [PubMed: 10570490]
- Guzowski JF, Timlin JA, Roysam B, McNaughton BL, Worley PF, Barnes CA. Mapping behaviorally relevant neural circuits with immediate-early gene expression. *Curr Opin Neurobiol*. 2005; 15:599–606. [PubMed: 16150584]
- Johnson BA, Frostig RD. Photonics meets connectomics: case of diffuse, long-range horizontal projections in rat cortex. *Neurophotonics*. 2015; 2:041403. [PubMed: 26158017]
- Kim Y, Venkataraju KU, Pradhan K, Mende C, Taranda J, Turaga SC, Arganda-Carreras I, Ng L, Hawrylycz MJ, Rockland KS, Seung HS, Osten P. Mapping social behavior-induced brain activation at cellular resolution in the mouse. *Cell reports*. 2015; 10:292–305. [PubMed: 25558063]
- Klein A, Andersson J, Ardekani BA, Ashburner J, Avants B, Chiang MC, Christensen GE, Collins DL, Gee J, Hellier P, Song JH, Jenkinson M, Lepage C, Rueckert D, Thompson P, Vercauteren T, Woods RP, Mann JJ, Parsey RV. Evaluation of 14 nonlinear deformation algorithms applied to human brain MRI registration. *Neuroimage*. 2009; 46:786–802. [PubMed: 19195496]
- Kulkarni PM, Barton E, Savelonas M, Padmanabhan R, Lu Y, Trett K, Shain W, Leasure JL, Roysam B. Quantitative 3-D analysis of GFAP labeled astrocytes from fluorescence confocal images. *J Neurosci Methods*. 2015; 246:38–51. [PubMed: 25745860]
- Leergaard TB, Lakke EA, Bjaalie JG. Topographical organization in the early postnatal corticopontine projection: a carbocyanine dye and 3-D computer reconstruction study in the rat. *J Comp Neurol*. 1995; 361:77–94. [PubMed: 8550883]
- Meghani M, Rey-Villamizar N, Merouane A, Lu Y, Mukherjee A, Trett K, Chong P, Harris C, Shain W, Roysam B. Population-scale three-dimensional reconstruction and quantitative profiling of microglia arbors. *Bioinformatics (Oxford, England)*. 2015; 31:2190–8.
- Mitra, P., Bokil, H. *Observed Brain Dynamics*. Oxford University Press; New York: 2007.
- Montes-Rodriguez CJ, Lapointe V, Trivedi V, Lu Q, Demchuk AM, McNaughton BL. Postnatal development of *Homer1a* in the rat hippocampus. *Hippocampus*. 2013; 23:890–902. [PubMed: 23733398]
- Narayanaswamy A, Wang Y, Roysam B. 3-D image pre-processing algorithms for improved automated tracing of neuronal arbors. *Neuroinformatics*. 2011; 9:219–31. [PubMed: 21537877]
- Oh SW, Harris JA, Ng L, Winslow B, Cain N, Mihalas S, Wang Q, Lau C, Kuan L, Henry AM, Mortrud MT, Ouellette B, Nguyen TN, Sorensen SA, Slaughterbeck CR, Wakeman W, Li Y, Feng D, Ho A, Nicholas E, Hirokawa KE, Bohn P, Joines KM, Peng H, Hawrylycz MJ, Phillips JW, Hohmann JG, Wornoutka P, Gerfen CR, Koch C, Bernard A, Dang C, Jones AR, Zeng H. A mesoscale connectome of the mouse brain. *Nature*. 2014; 508:207–14. [PubMed: 24695228]
- Paxinos, G., Watson, C. *The rat brain in stereotaxic coordinates*. 4. Academic Press; New York: 2007.
- Peng H, Bria A, Zhou Z, Iannello G, Long F. Extensible visualization and analysis for multidimensional images using Vaa3D. *Nat. Protocols*. 2014a; 9:193–208. [PubMed: 24385149]
- Peng H, Tang J, Xiao H, Bria A, Zhou J, Butler V, Zhou Z, Gonzalez-Bellido PT, Oh SW, Chen J, Mitra A, Tsien RW, Zeng H, Ascoli GA, Iannello G, Hawrylycz M, Myers E, Long F. Virtual

finger boosts three-dimensional imaging and microsurgery as well as terabyte volume image visualization and analysis. *Nat Commun.* 2014b; 5

- Petrovich GD, Holland PC, Gallagher M. Amygdalar and prefrontal pathways to the lateral hypothalamus are activated by a learned cue that stimulates eating. *J Neurosci.* 2005; 25:8295–302. [PubMed: 16148237]
- Ragan T, Kadiri LR, Venkataraju KU, Bahlmann K, Sutin J, Taranda J, Arganda-Carreras I, Kim Y, Seung HS, Osten P. Serial two-photon tomography for automated ex vivo mouse brain imaging. *Nat Meth.* 2012; 9:255–8.
- Rey-Villamizar N, Somasundar V, Meghani M, Xu Y, Lu Y, Padmanabhan R, Trett K, Shain W, Roysam B. Large-scale automated image analysis for computational profiling of brain tissue surrounding implanted neuroprosthetic devices using Python. *Front Neuroinform.* 2014; 8:39. [PubMed: 24808857]
- Sage D, Prodanov D, Tinevez J-Y, Schindelin J. MIJ: Making Interoperability Between ImageJ and Matlab Possible ImageJ User & Developer Conference (IUDC'12). Luxembourg. 2012
- Schindelin J, Arganda-Carreras I, Frise E, Kaynig V, Longair M, Pietzsch T, Preibisch S, Rueden C, Saalfeld S, Schmid B, Tinevez J-Y, White DJ, Hartenstein V, Eliceiri K, Tomancak P, Cardona A. Fiji: an open-source platform for biological-image analysis. *Nat Meth.* 2012; 9:676–82.
- Sorns O. Contributions and challenges for network models in cognitive neuroscience. *Nat Neurosci.* 2014; 17:652–60. [PubMed: 24686784]
- Van Essen DC. Cartography and connectomes. *Neuron.* 2013; 80:775–90. [PubMed: 24183027]
- Vazdarjanova A, McNaughton BL, Barnes CA, Worley PF, Guzowski JF. Experience-dependent coincident expression of the effector immediate-early genes arc and Homer 1a in hippocampal and neocortical neuronal networks. *J Neurosci.* 2002; 22:10067–71. [PubMed: 12451105]
- Vousden DA, Epp J, Okuno H, Nieman BJ, van Eede M, Dazai J, Ragan T, Bito H, Frankland PW, Lerch JP, Henkelman RM. Whole-brain mapping of behaviourally induced neural activation in mice. *Brain structure & function.* 2015; 220:2043–57. [PubMed: 24760545]
- Watabe-Uchida M, Zhu L, Ogawa Sachie K, Vamanrao A, Uchida N. Whole-Brain Mapping of Direct Inputs to Midbrain Dopamine Neurons. *Neuron.* 2012; 74:858–73. [PubMed: 22681690]
- Wilber AA, Clark BJ, Demecha A, Mesina L, Vos J, McNaughton BL. Automated cortical connectivity maps reveal anatomically distinct areas in the parietal cortex of the rat. *Frontiers in Neural Circuits.* 2015; 8:1–15.
- Wilber AA, Clark BJ, Forster TC, Tatsuno M, McNaughton BL. Interaction of Egocentric and world centered reference frames in the rat posterior parietal cortex. *J. Neurosci.* 2014; 34:5431–46. [PubMed: 24741034]
- Zelikowsky M, Bissiere S, Hast TA, Bennett RZ, Abdipranoto A, Vissel B, Fanselow MS. Prefrontal microcircuit underlies contextual learning after hippocampal loss. *Proc Natl Acad Sci U S A.* 2013; 110:9938–43. [PubMed: 23676273]
- Zingg B, Hintiryan H, Gou L, Song Monica Y, Bay M, Bienkowski Michael S, Foster Nicholas N, Yamashita S, Bowman I, Toga Arthur W, Dong H-W. Neural Networks of the Mouse Neocortex. *Cell.* 2014; 156:1096–111. [PubMed: 24581503]

### Highlights

- A novel software platform is presented for the large-scale assessment of gene expression and neural connectivity in the rodent brain.
- The presented toolkit was developed in Matlab and utilizes open-source and custom platforms to accommodate a largely automated analysis pipeline in which an investigator can visualize and quantify whole brain data in 3-D, and can be rapidly integrated with user-specific analyses and methodologies.

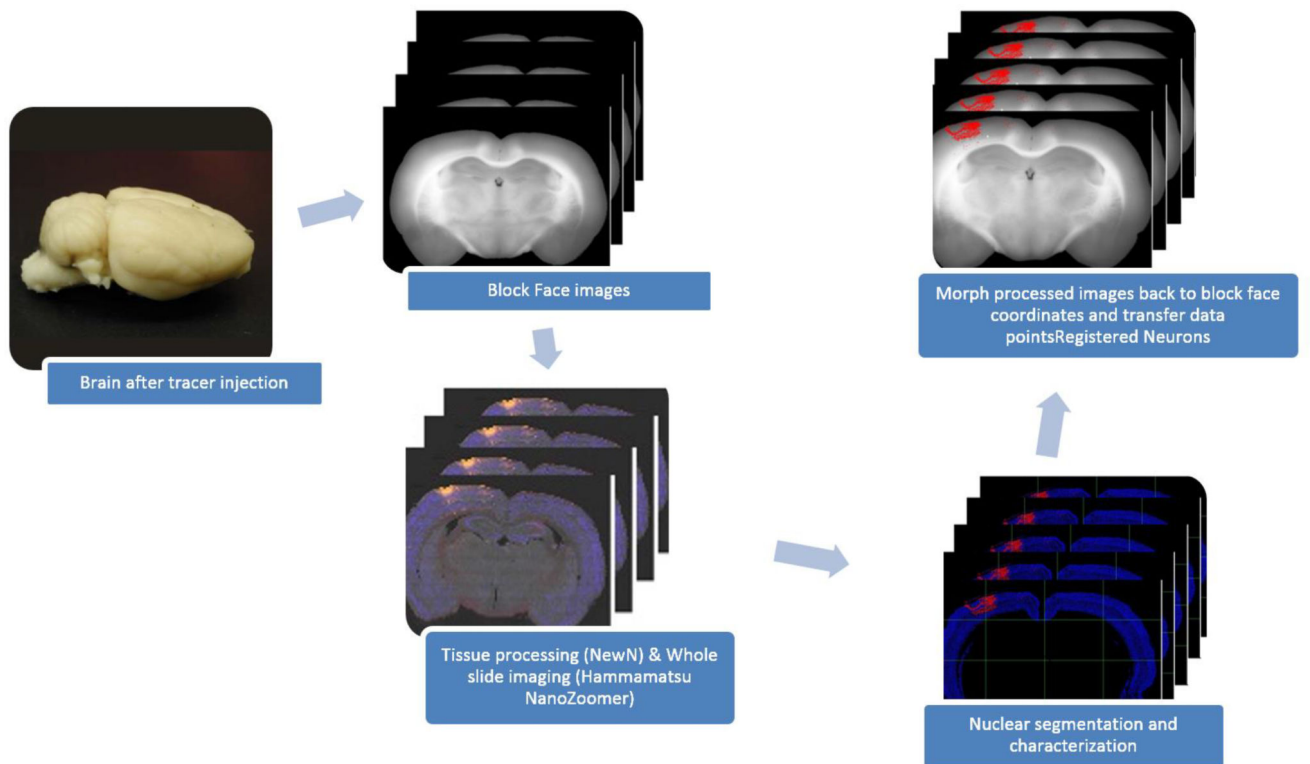


**Figure 1.** Pipeline for whole-brain assessment of neural connectivity. Block-face images provide an un-distorted whole brain reference coordinate system.

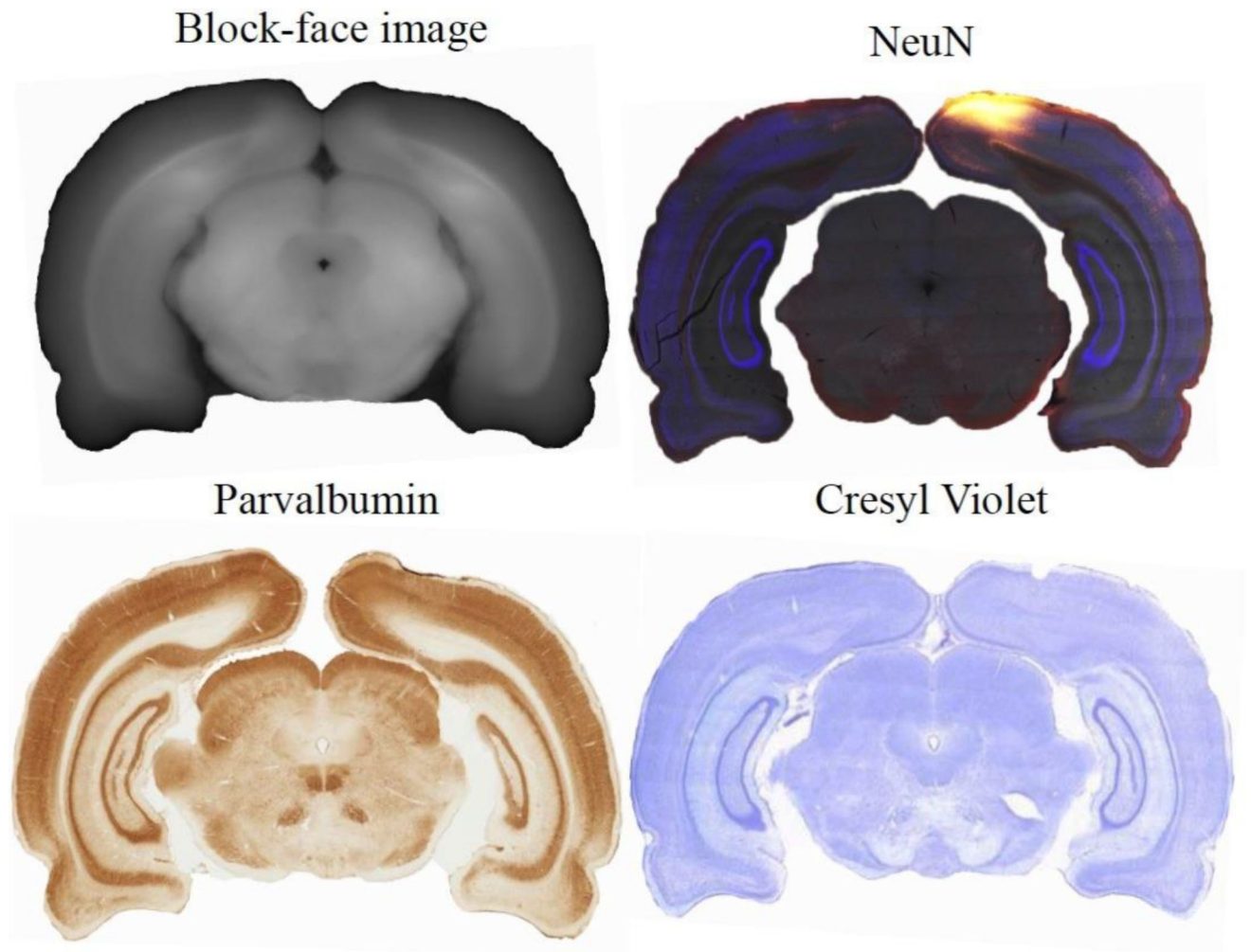


**Figure 2.** Histological processing. An image was taken of each section just prior to sectioning (Block-face image). Then each section was processed for either the neuronal marker (NeuN) for neuronal segmentation and automatic detection of tracer filled cells, or with a stain to aid in identification of regional boundaries (Parvalbumin or Cresyl Violet).

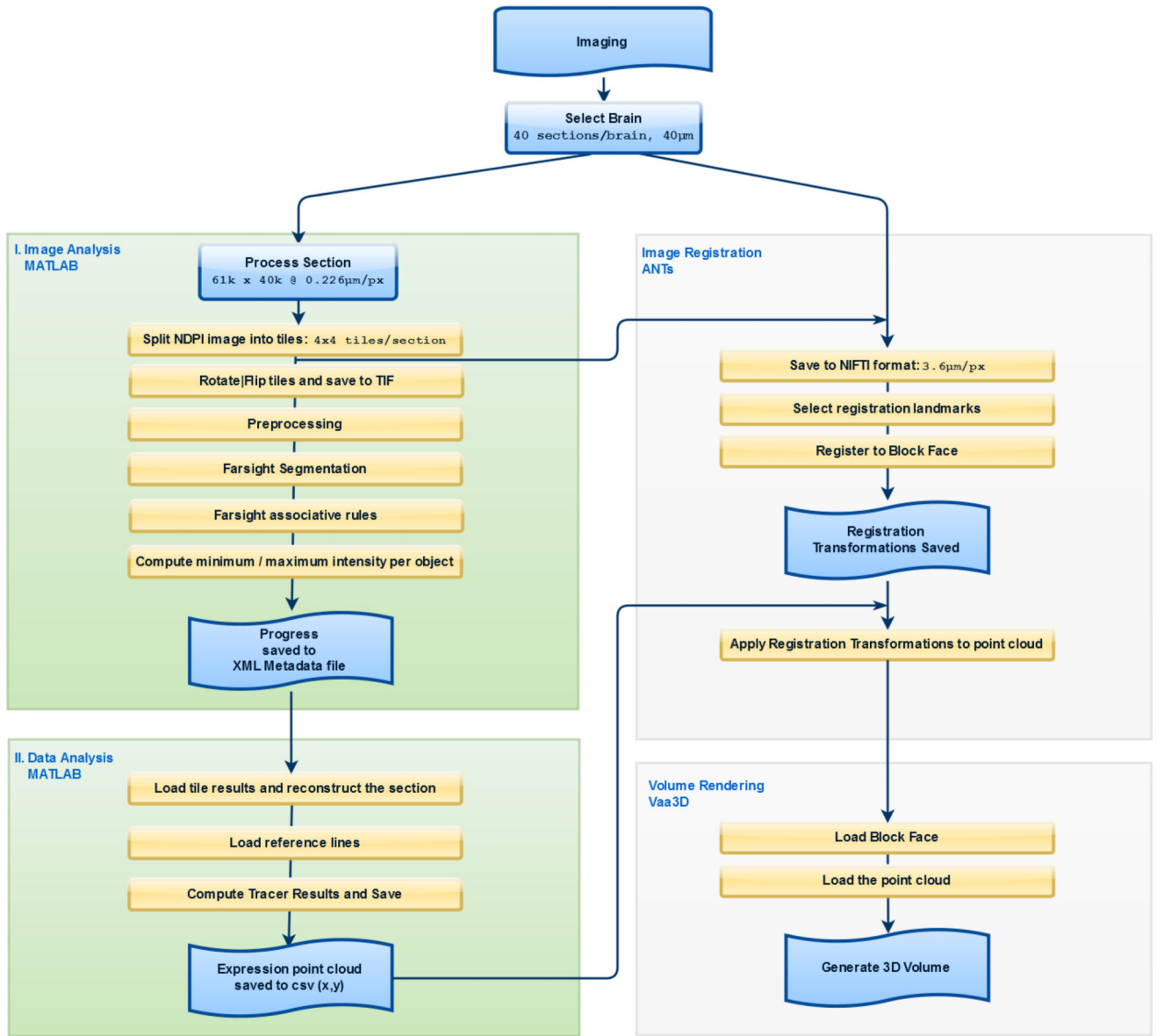


**Figure 3.** Workflow diagram. Processing is orchestrated with the Matlab GUI (in green). High-resolution whole section images are processed in two divided segments, allowing the user to run Image Analysis on the tiles and extract data from the image and then perform Data Analysis on very large datasets. ANTs permits registration computations and transformations which are applied to the point cloud. Finally the points cloud and block face image are used to generate the 3D volume rendering in Vaa3D. Vaa3D, is the only efficient software currently available for rendering very large datasets of this type. Note this workflow illustrates the process for a single section. This is repeated for each section, then all registered points data is assembled into a single CSV file.

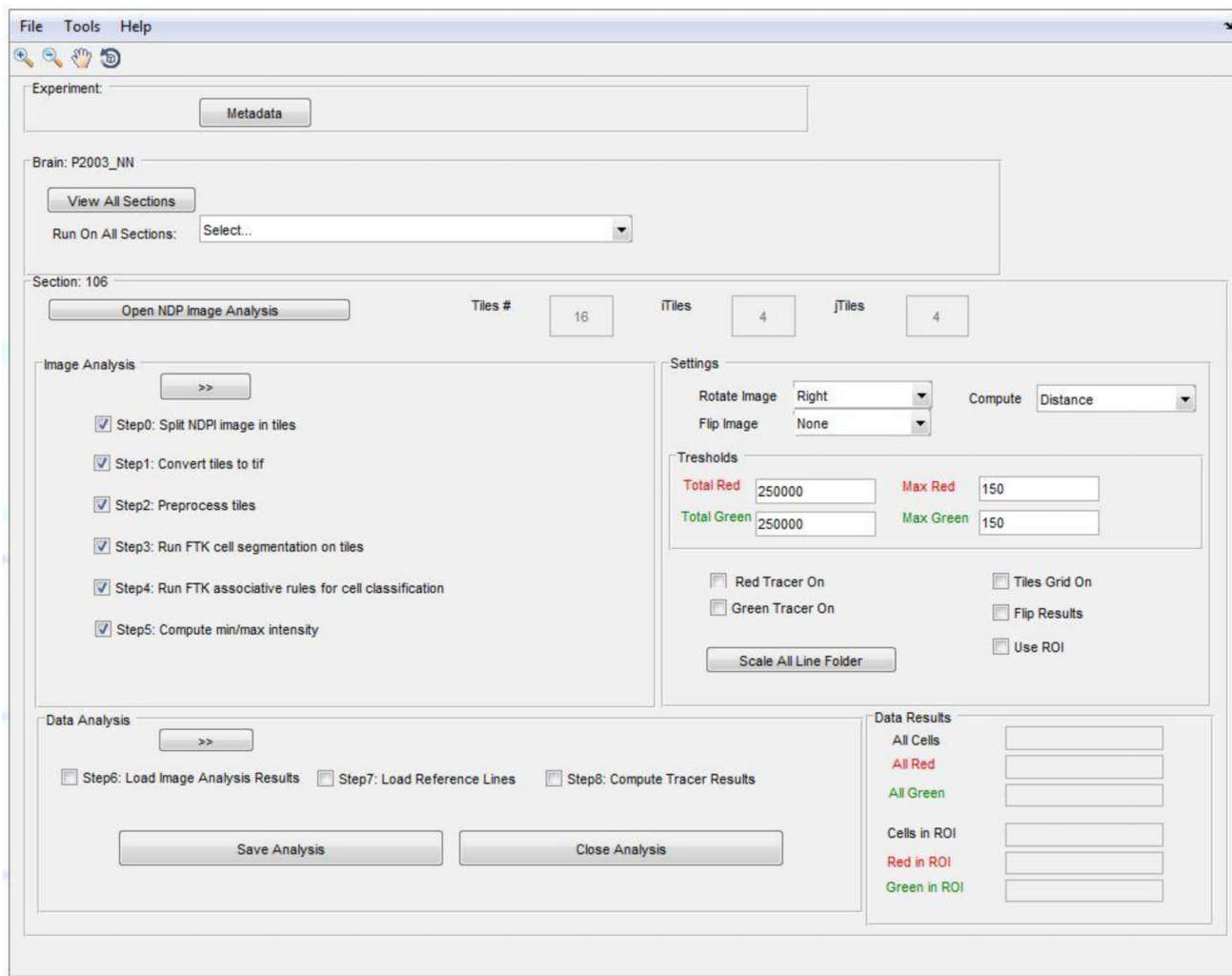
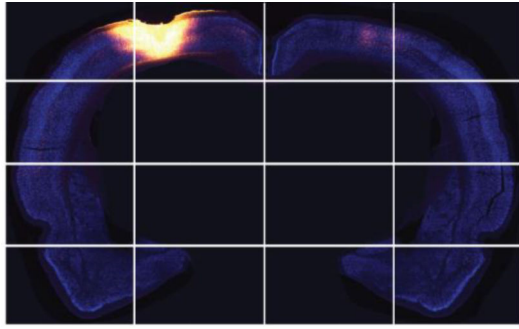
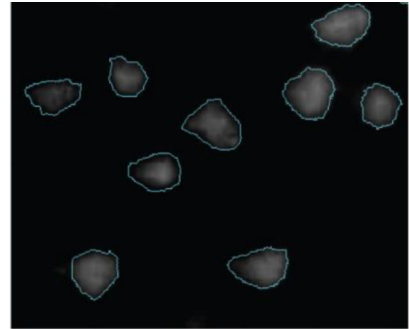


**Figure 4.** Overview of the Matlab Graphical User Interface. The platform allows the user to run the analysis steps in two separate modes (see Figure 3). The analysis workflow is broken down into manageable groups (see green boxes on Figure 3) and then into manageable steps within the groupings (step 0–5 and 6–8). Tiles are by default processed in batch mode. In this example, section 106 has the first analysis group (Image Analysis) completed and the user can proceed with ‘Data Analysis’. All the processing progress is saved in the background to a XML Metadata file, which streamlines and automates progress tracking. The Matlab GUI accommodates the problems inherent when working with large data sets by extracting information from the image tiles, then assembly and work only with the extracted data.





High resolution (40x magnification) tile images are created and saved.



Neuronal segmentation using Farsight Toolkit

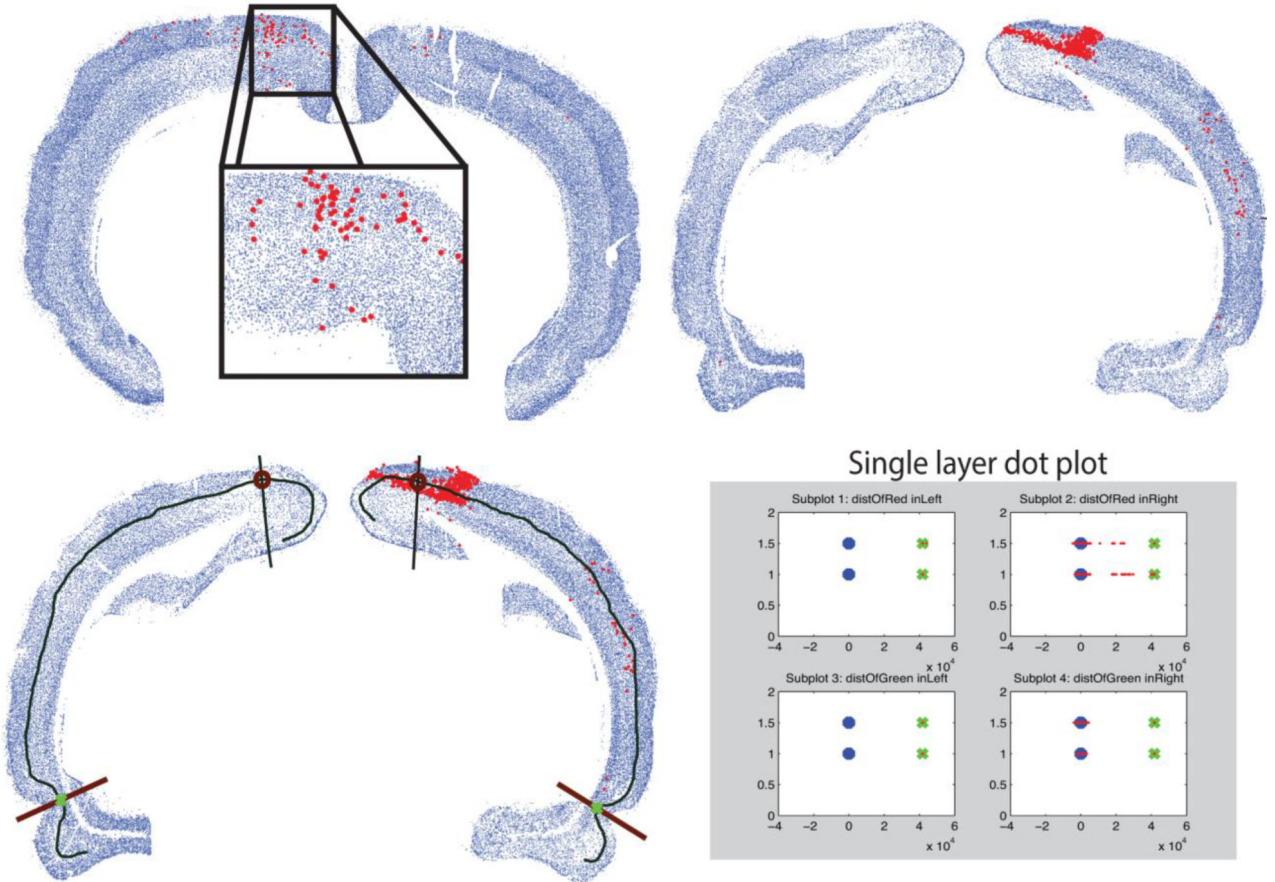


**Figure 5.** Tools for automated tracer detection and semi-automatic whole brain cortical flat maps. High resolution images are tiled to a manageable size (top left), then individual neuronal marker stained neurons are automatically segmented on each cortical tile (top right). Next cells with enough tracer to cross the user specified threshold (middle) are automatically identified. Finally, the user has the option to either quantify data for a region of interest or generate a cortex wide flat map automatically by marking off two reference points (e.g., rhinal sulcus and cingulum border) and drawing a line through a specific cortical layer.

Author Manuscript

Author Manuscript

Author Manuscript

Author Manuscript

Finally data are automatically classified by distance along the cortex line and separately for the labeled cells that reside above versus below the cortex line.

Author Manuscript

Author Manuscript

Author Manuscript

Author Manuscript

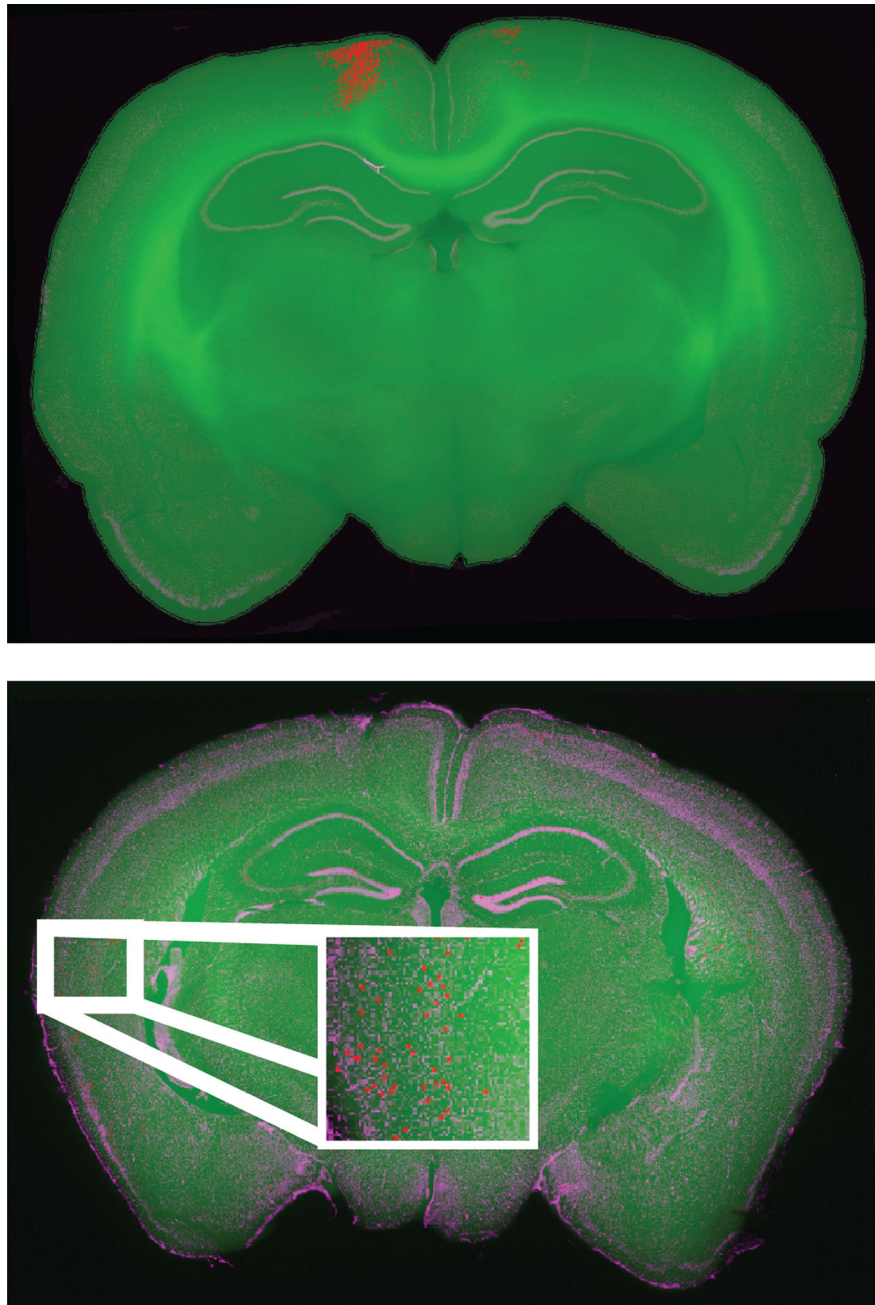


**Figure 6.** Example of fully automated registration for a rat brain (top) with automated quantification of a retrograde tracer (red) and for a mouse brain (bottom) with automatically identified IEG expressing cells (red). Automated registration alone was sufficient to produce good alignment of histologically processed tissue (grey for rat brain or purple for mouse brain) to the block face image. However, for a small number of sections in the region of the hippocampus an additional step of points based registration was necessary (not shown).

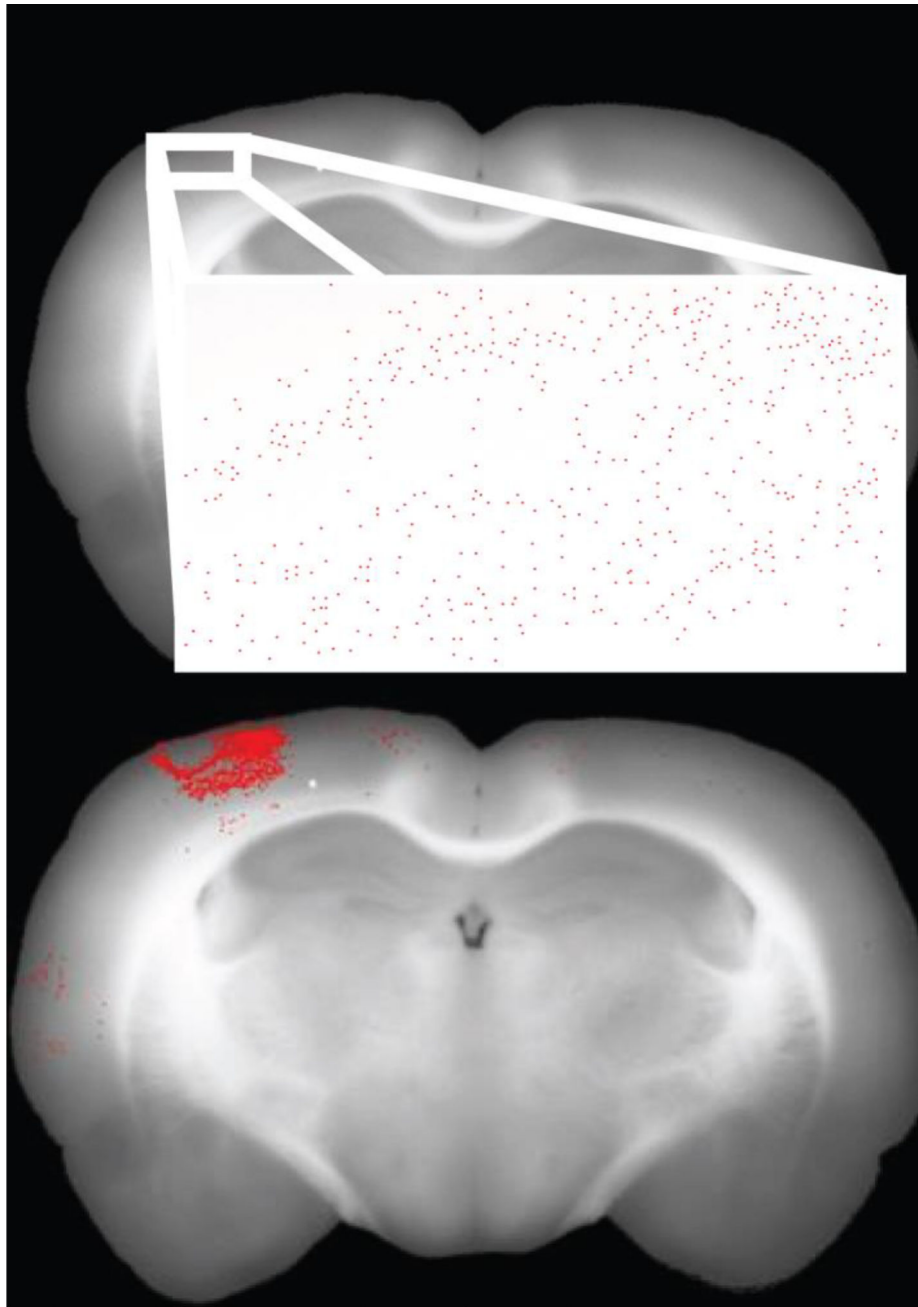


**Figure 7.**

Data visualization and analysis formats.. Registered data can be stored in one of two formats, either with a single pixel colored to represent a “positive” cell (top) or with a large marker covering many pixels and indicating the location of “positive” cells (bottom). The larger markers are easier to see and thus ideal for subjective viewing of registered data. The single colored pixel method is ideal for data analyses and quantification because both the precise location of a “positive” cell and the number of positive cells (as pixels) are all directly available in high resolution and in the single image file for the tissue section.

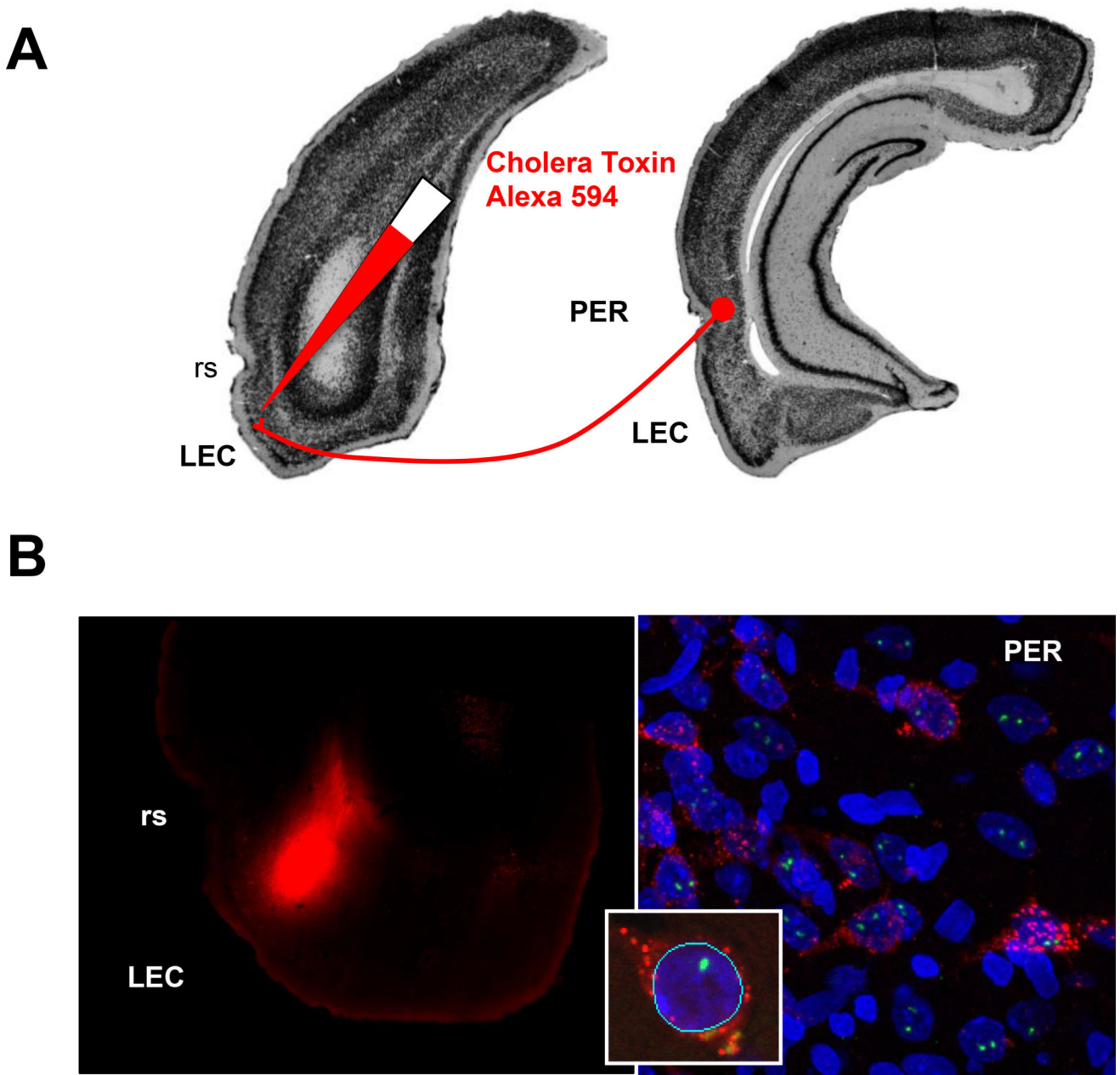


**Figure 8.**

A. Illustration showing protocol for retrograde tracer injection into the entorhinal cortex (left) and assessment of labeled cells in the perirhinal cortex (right). B. Left panel shows injection site within the lateral entorhinal cortex and the right panel shows double-labeled cells with retrograde tracer (red) and stained cell nuclei with DAPI (blue), and H1a labeling (green). Imaging was produced using NanoZoomer (B, left) and confocal microscopy (B, right) as described previously (Montes-Rodriguez et al., 2012). The inset shows an example nuclei segmented using FARSIGHT. Cells with both tracer and H1a labeling can be automatically detected by measuring the red channel integrated intensity just outside the

segmented boundary of the cell and measuring the green channel integrated intensity within the segmented nuclei.

Author Manuscript

Author Manuscript

Author Manuscript

Author Manuscript